Supporting Information for

Encapsulation of Crystalline and Amorphous Sb_2S_3 within Carbon and Boron Nitride Nanotubes

Griffin M. Milligan,[1] Dmitri Leo Mesoza Cordova,[1] Ze-Fan Yao,[2] Brian Y. Zhi,[1] Lyndsey R. Scammell,[3] Toshihiro Aoki,[4] Maxx Q. Arguilla[1]*

[1]Department of Chemistry, University of California Irvine; Irvine, California 92697, USA

[2]Department of Chemical and Biomolecular Engineering, University of California Irvine; Irvine, California 92697, USA

[3]BNNT LLC, 300 Ed Wright Lane Suite A, Newport News, Virginia 23606, United States

[4]Irvine Materials Research Institute, University of California Irvine; Irvine, California 92697, USA

*Corresponding author. Email: marguill@uci.edu

1. Materials and Methods

General Methods. Structures were generated in SingleCrystal 4 software (CrystalMaker® Software Suite). Carbon nanotubes were generated in Avogadro: an open-source molecular builder and visualization tool. Version 1.2.0. http://avogadro.cc/,[1] while boron nitride nanotubes were generated in VMD.[2] Calibrated optical images of representative crystals were taken with a Google Pixel 6. All figures were lay-outed and processed in Lunacy.

Synthesis of bulk Sb_2S_3 Precursors. Elemental precursors of antimony (99.5 %) and sulfur (99+%) were purchased from STREM and used without further purification. Bulk Sb_2S_3 crystals that were used as precursors for subsequent syntheses were grown as follows: Stoichiometric quantities of Sb and S (2:3 ratio) were evacuated in quartz ampoules (10 mm I.D.; 12 mm O.D.) under a <50 mTorr base pressure and were subsequently flame sealed. The ampoules were then uniformly heated to 600 °C for 96 hours in a single-zone vertical tube furnace (OTF-1200F; MTI Inc.) then cooled over the course of 48 hours. The phase purity of the Sb_2S_3 polycrystals were confirmed by powder X-ray diffraction (PXRD) on a Rigaku MiniFlex diffractometer (**Fig. S1**). The resulting diffractogram was compared to the reported literature structure.[3]

Encapsulation of Sb_2S_3 within SWCNTs, MWCNTs, & BNNTs. High purity single-walled carbon nanotubes (1.6 ± 0.4 nm diameter, Tuball, OCSiAl) were opened by heating the as-received nanotubes at 420 °C in ambient air conditions for five hours. 10-20 nm multi-walled carbon nanotubes (Cheap Tubes Inc.) were heat treated at 420 °C for five to ten hours. Purified and treated (to open the ends) boron nitride nanotubes (BNNT LLC) were filled with Sb_2S_3 without an oxidation step. A calcination step at 800 °C or stirring in aqua regia (3:1 conc. HCl/conc. HNO_3) was found to make no considerable difference. Approximately 5 mg of these pre-treated NTs were then loaded into quartz ampoules immediately after heat treatment (10 mm I.D.; 12 mm O.D.) and mixed with a large excess of powdered Sb_2S_3 polycrystals, ranging from 200 to 300 mg. Ampoules containing NTs and Sb_2S_3 powders were evacuated under vacuum <50 mTorr and were immediately flame sealed. The ampoules were then heated to 600 °C for 96 hours in a single-zone vertical tube furnace (OTF-1200F; MTI Inc.) then cooled over the course of 48 hours. After the reaction, the Sb_2S_3@NTs were found to have phase separated from the Sb_2S_3 melt. The Sb_2S_3@NTs were physically isolated from the resulting Sb_2S_3 boule and were used in the succeeding experiments without further purification. Prior to ensemble measurements, the as-synthesized samples were washed and purified using isopropanol *via* a mixture of gentle pipetting, vortex mixing, and bath sonication and dried in a vacuum oven at 80 °C for at least one hour.

High-resolution transmission electron microscopy (HRTEM), scanning transmission electron microscopy (STEM), and elemental mapping. The resulting Sb_2S_3@NT heterostructures were dispersed in isopropanol (*i*-PrOH, 99.8%, Fisher Scientific) first gently suspending manually by pipetting several times before bath sonication for 5 mins, then drop-casted onto lacey carbon grids (Lacey Formvar/Carbon, 200 mesh, Cu grid; Ted Pella, Inc.) HRTEM images were acquired using a JEOL JEM-2800 S/TEM operated at an accelerating voltage of 200 kV equipped with a Gatan OneView 4K camera with drift correction. EDS mapping of Sb_2S_3@BNNTs was performed with the same microscope in STEM mode using dual 100 mm^2 Si drift detectors. C_s-corrected scanning transmission electron microscopy (STEM) images and energy-dispersive X-ray spectra (EDS) of Sb_2S_3@SWCNTs was collected using a JEOL JEM-ARM300F Grand Arm electron microscope also equipped with dual 100 mm^2 Si drift detectors operated at 80 kV. Post-processing and image analyses of raw HRTEM and STEM data (.dm4) were done in Digital Micrograph (Gatan). Fast Fourier transform (FFT) analyses of the micrographs were done in Fiji.[4] Indexing of the FFT data were performed by comparing the experimental patterns with simulated patterns of the bulk single crystal structure using the SingleCrystal 4 software (CrystalMaker® Software Suite). HRTEM images were simulated using clTEM.[5]

Raman Spectroscopy. Raman spectra were collected on a Horiba LabRAM HR Evolution with a 532 nm laser. Samples were prepared by dispersing Sb_2S_3@NTs in *i*-PrOH, sonicating for 5 to 20 mins, then drop-casting onto

SiO_2/Si substrate. Carbon nanotube G-bands were assessed by peak fitting in MagicPlot Pro with two Lorentzian peaks and a spline background. Peak maxima of filled and empty MWCNTs and SWCNTs were extracted and compared. The broadening of the G-bands was assessed by extracting the full width at half maximum (FWHM) of each peak.

Diffuse Reflectance Spectroscopy (DRS). Composite samples for DRS measurements were prepared by individually grinding Sb_2S_3@NTs, empty NTs, and bulk Sb_2S_3 crystals with spectroscopic grade potassium bromide (KBr, >99% trace metal basis, Sigma Aldrich). These dilute samples were packed and compressed onto a custom-made holder with a transparent quartz window. DRS measurements on these as-prepared samples were performed on a Jasco V-670 spectrometer equipped with a 60 mm integrating sphere (Jasco ISN-923) which operates at a working range of 190-2500 nm. The resulting diffuse reflectance spectra were converted using the Kubelka-Munk function ($F(R_\infty)$) to approximate the absorbance profiles of the samples.[6]

Ultraviolet-Visible (UV-Vis) Absorbance Spectroscopy. Individual suspensions of Sb_2S_3@BNNTs and empty BNNTs were prepared by sonicating the samples in *i*-PrOH for 5-20 mins. Immediately after sonication, room temperature absorption spectra of the resulting suspensions in the 200 nm to 800 nm range were collected using Agilent Cary 100 UV-Vis spectrophotometer. Pure *i*-PrOH was used as a blank solution for these measurements.

First-principles density functional theory calculations of the Sb_2S_3@SWCNT$_{(21,0)}$ and Sb_2S_3@SWBNNT$_{(21,0)}$ heterostructures. DFT calculations were performed to determine the electron density difference map of a single chain of Sb_2S_3 encapsulated within a (21,0) zig-zag SWCNT and SWBNNT. This (n,m) index falls within the suitable diameter (~1.6 nm) experimentally observed to house single covalent chains of Sb_2S_3. All DFT calculations were conducted using the Cambridge Serial Total Energy Package, CASTEP academic 22.11 release.[7] Generalized gradient approximation (GGA) with Perdew-Burke-Ernzerhof (PBE) parametrization and Grimme's DFT-D2 van der Waals force correction were used with on-the-fly generation (OTFG) ultrasoft pseudopotentials.[8,9] Real-space mesh cut-off of 550 eV was used for all DFT calculations. A periodic-boundary-condition (PBC) supercell of a single chain of Sb_2S_3 in a (21,0) SWCNT or SWBNNT was built where the long-axis ([010] direction) of the Sb_2S_3 chain was aligned to the *z*-axis of the CNT. The supercells that were constructed consisted of two-unit cell lengths along the crystallographic [010] direction of the Sb_2S_3 crystal structure to minimize the incommensurate lattice mismatch between the Sb_2S_3 and the SWCNT/SWBNNT. The supercell system was then energy minimized using Monkhorst-Pack *k*-point mesh at Gamma until the total energies converged to 10^{-5} eV per atom and displacements less than 0.001 Å. The electron density difference map was calculated using the optimized geometry with Monkhorst-Pack *k*-point mesh of 1×1×15. Bader atomic charges of the systems were calculated using electron density from the final single-point CASTEP calculation with the help of den2VASP and Bader charge analysis codes.[10,11]

X-Ray Photoelectron Spectroscopy (XPS). XPS samples were prepared by adhering a large quantity of nanotubes (in the case of Sb_2S_3@SWCNT, Sb_2S_3@BNNT, SWCNT, and BNNT) or single crystals of Sb_2S_3 to a plane dual height holder with carbon tape. Spectra were collected on a Kratos Analytical Axis Supra with an Al/Ag monochromated X-ray source and charge neutralizer. Peaks were fit in CasaXPS software using a spline Shirley background and asymmetric Lorentzian peaks. Samples without CNTs were calibrated to adventitious carbon 1s at 284.8 eV, while CNT rich samples were calibrated to the strong graphitic C=C peak at 284.5 eV.[12]

Thermogravimetric Analysis (TGA). TGA was collected on a TA Instruments TGA Q500 with a nitrogen purge at a ramp rate of 20 °C/min from room temperature to 1000 °C.

Electrical Measurements. Samples were pressed into pellets at 14 MPa between circular disks cut from a weigh boat to aid in liftoff. Rectangular sections (Sb_2S_3@BNNT: l=0.168 cm, A=0.269 x 0.0295 cm = 0.00796 cm^2; empty BNNT: l=0.136 A=0.264 x 0.0242 cm = 0.00637 cm^2) taken from these pellets and were contacted with pressed indium contacts. Current-voltage (I-V) curves and time-dependent current profiles measured with a forward bias of

10 V were measured using a probe station equipped with a Keithley 4200 SCS semiconductor parameter analyzer. For photocurrent generation measurements, the fabricated devices were illuminated by a Prizmatix 415-nm FC-LED light source at 13 mW/cm^2 controlled by a programmable pulse generator at 0.5 Hz with a 1 s exposure time.

2. Supplementary Data and Results

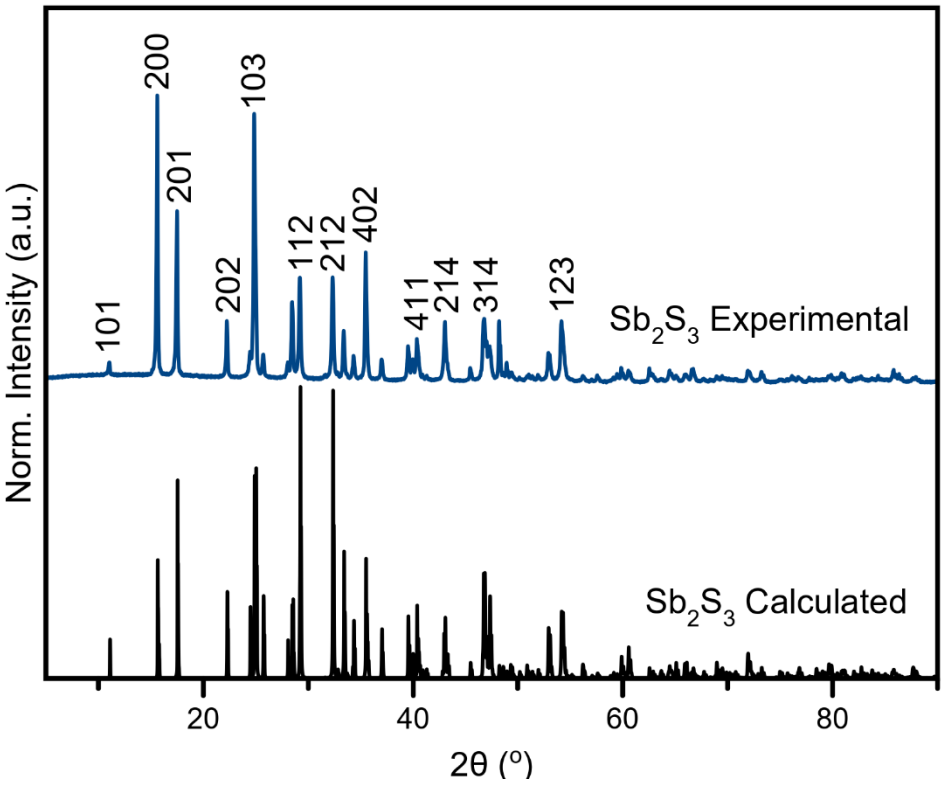

Figure S1. PXRD of bulk Sb_2S_3 powder used to fill MWCNTs, SWCNTs, and BNNTs in the study.

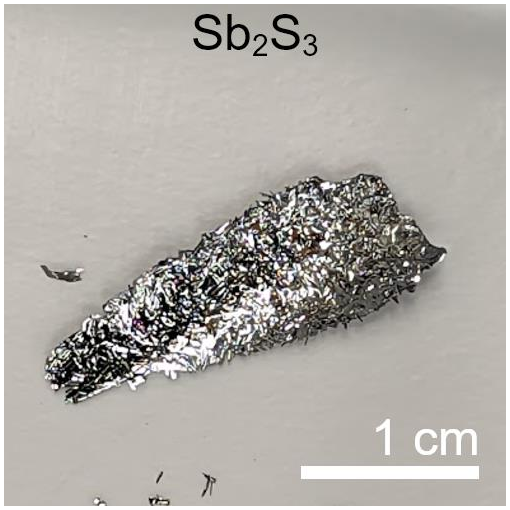

Figure S2. Optical image of gray Sb_2S_3 polycrystals used to fill carbon and boron nitride nanotubes.

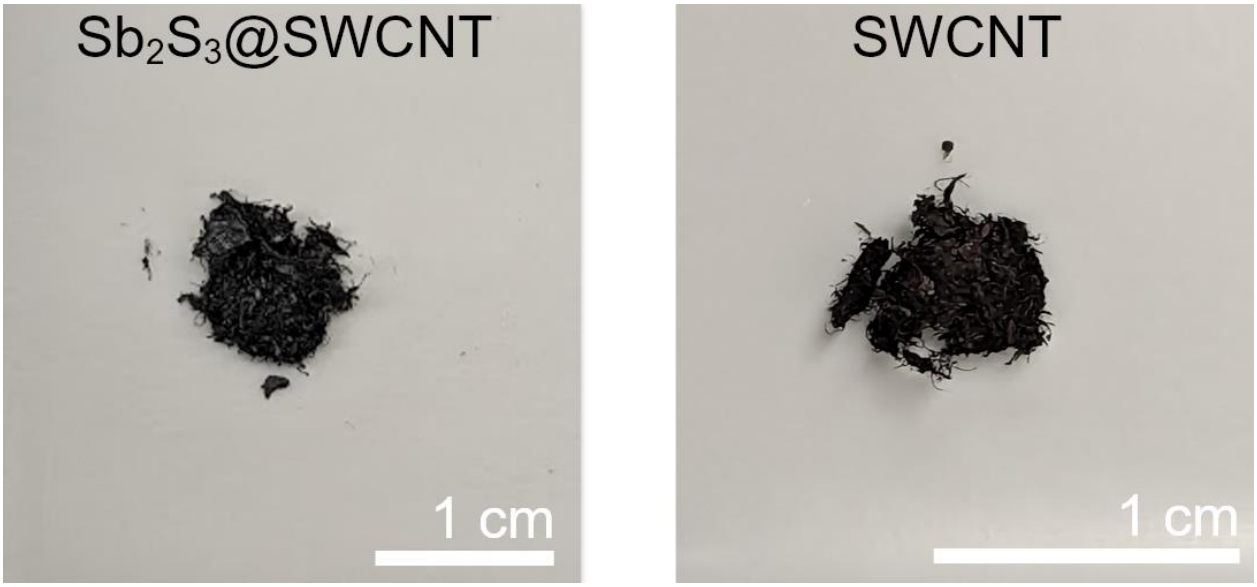

Figure S3. Optical image of black Sb_2S_3@SWCNTs (left) and black empty SWCNTs fibers (right).

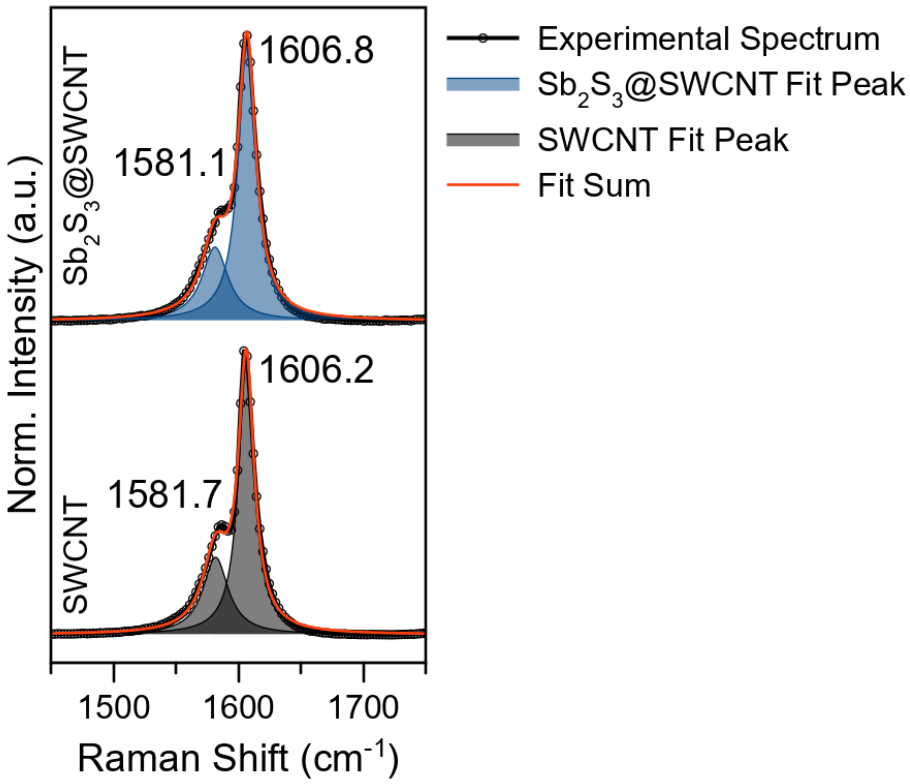

Figure S4. Raman peak fit of G-band region of Sb_2S_3@SWCNT and SWCNT spectrum with negligible shifts and negligible peak broadening.

Table S1. FWHM values of fitted Raman peaks from **Fig. S4**.

Sample	**Peak Position (cm^{-1})**	**FWHM (cm^{-1})**
Sb_2S_3@SWCNT G^-	1581.1 ± 0.4	25.7 ± 1.3
SWCNT G^-	1581.7 ± 0.3	24.6 ± 1.0
Sb_2S_3@SWCNT G^+	1606.8 ± 0.1	17.2 ± 0.3
SWCNT G^+	1606.2 ± 0.2	15.3 ± 0.2

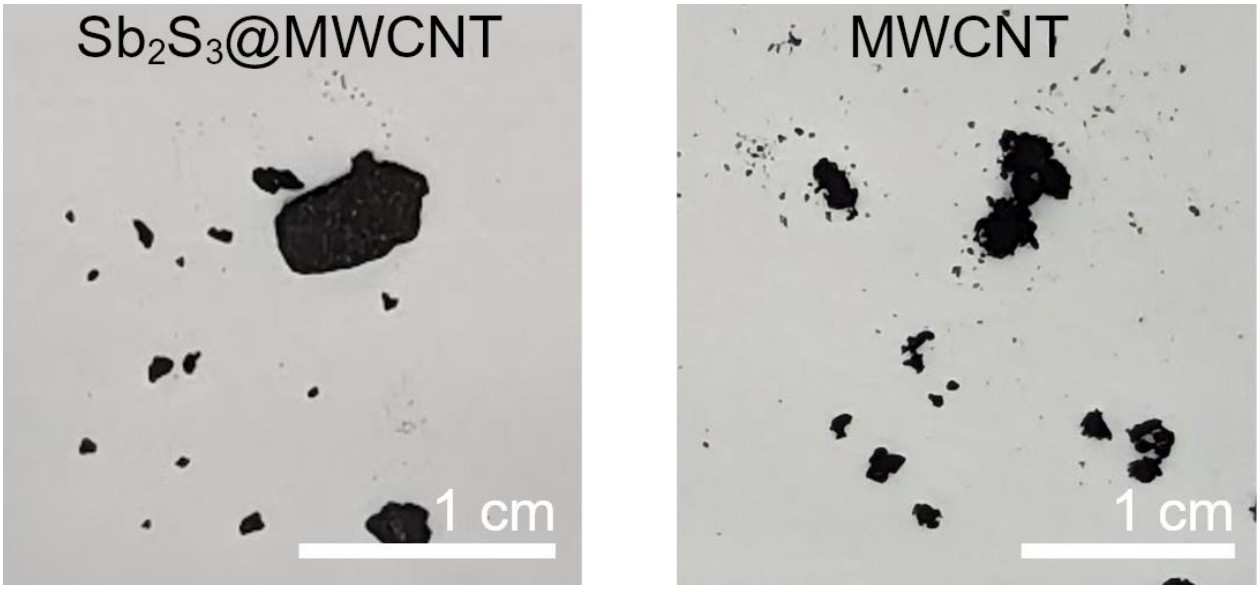

Figure S5. Optical images of black Sb_2S_3@MWCNT (left) and black empty MWCNT powders (right).

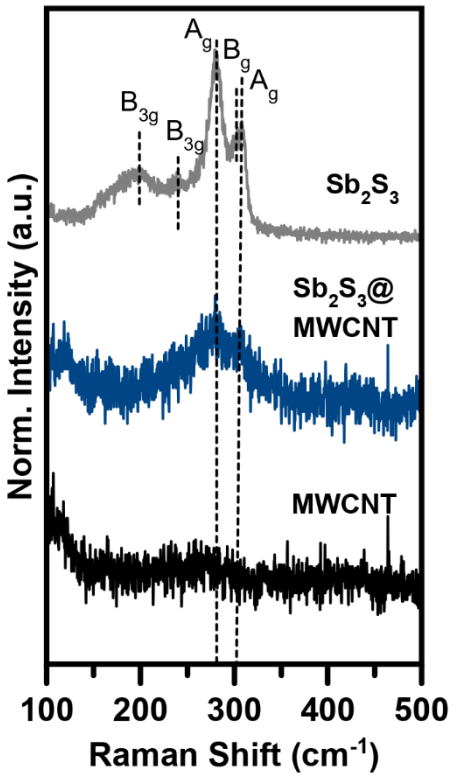

Figure S6. Raman spectrum of the low wavenumber region of Sb_2S_3@MWCNTs, Sb_2S_3, and MWCNTs showing both A_g peaks remain visible despite confinement effects.

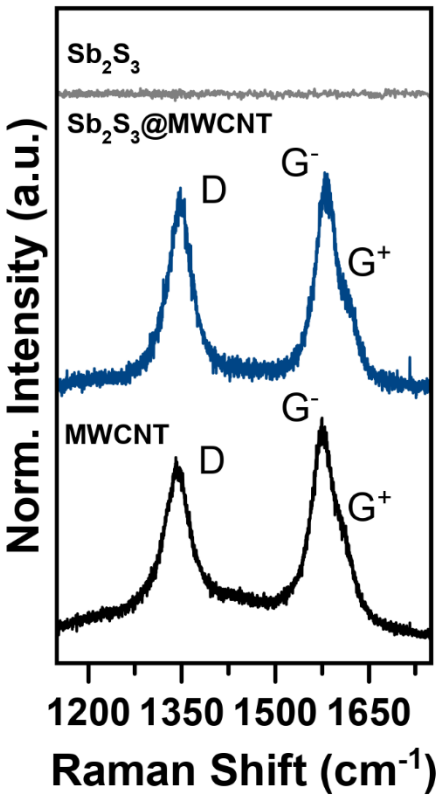

Figure S7. Raman spectrum of the high wavenumber region of Sb_2S_3@MWCNTs, Sb_2S_3, and MWCNTs.

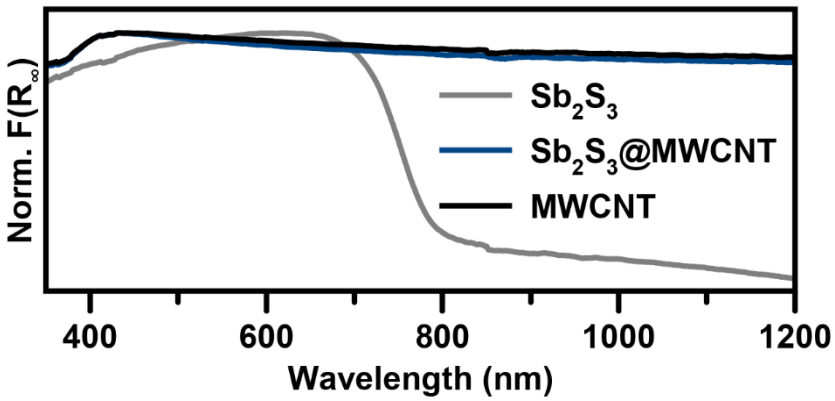

Figure S8. DRS of Sb_2S_3@MWCNTs, Sb_2S_3, and MWCNTs showing that, as with SWCNTs, broadband absorbance of MWCNTs create difficulties when attempting to measure the optical properties of a guest material.

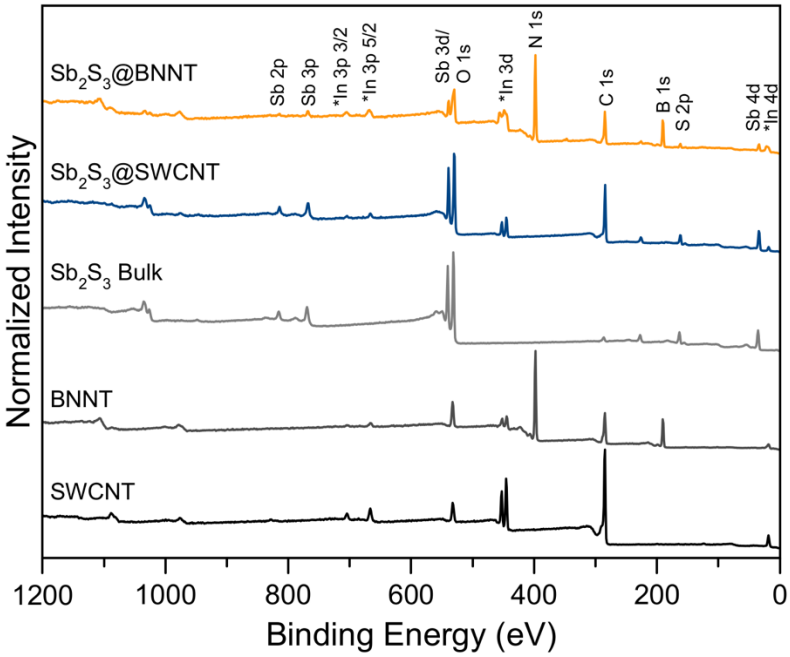

Figure S9. Wide range XPS survey of Sb_2S_3 in bulk and encapsulated form in BNNTs and SWCNTs. Initially, In powder (*) was spiked into the sample to serve as an external calibration as some samples contained carbon while others did not. Unfortunately, charge neutralizer overcompensation in insulating samples (Sb_2S_3 bulk crystal, empty BNNTs) calibrated to In *3d* displayed erratic values several eV above literature. Instead, following literature procedures, samples that did not contain graphitic carbon (a-Sb_2S_3@BNNT, Sb_2S_3, BNNTs) were calibrated to the C *1s* of the adventitious carbon peak at 284.8 eV while graphitic carbon-containing samples (c-Sb_2S_3@SWCNT, empty SWCNTs) were calibrated to the sharp C *1s* peak at 284.5 eV.[12] This calibration appeared to arrive at the most reasonable values and is consistent with literature for fitting of adventitious and graphitic carbon samples.

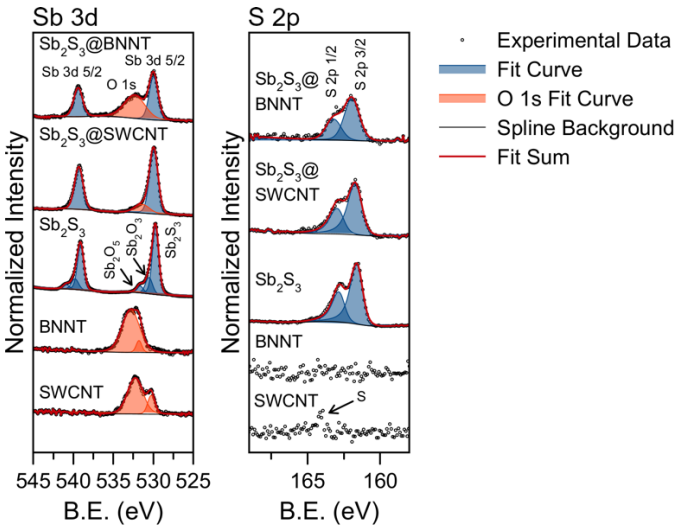

Figure S10. Regional XPS of Sb *3d* and S *2p* peaks. Sb $3d_{5/2}$ peaks overlap with O *1s*, which is colored red for clarity. It can be observed that only one Sb^{3+} environment is present in both the @BNNT and @SWCNT samples when compared to the three Sb types in bulk Sb_2S_3, which contains a prominent peak of Sb_2S_3 but also two Sb oxide peaks, one for Sb_2O_3 and one for Sb_2O_5. This indicates the nanotubes may offer some protection against oxidation at room temperature. Only one S environment is observed in a-Sb_2S_3@BNNT, c-Sb_2S_3@SWCNT, and bulk Sb_2S_3. Empty SWCNTs showed a minor S impurity peak likely from cross contamination during sample preparation.

Table S2 Fit XPS values of Sb 3d and S 2p.

Sb_2S_3@BNNT	Sb 3d 5/2	Sb 3d 3/2	S 2p 3/2	S 2p 1/2
Peak position (eV)	529.97	539.40	161.95	163.20
FWHM (eV)	1.3	1.3	1.24	1.24
Area	10580.5	7053.67	1209.82	604.91
Sb_2S_3@SWCNT	Sb 3d 5/2	Sb 3d 3/2	S 2p 3/2	S 2p 1/2
Peak position (eV)	529.95	539.31	161.67	162.92
FWHM (eV)	1.26	1.26	1.05	1.05
Area	41908.22	27938.81	4137.23	2068.61
Sb_2S_3 Bulk	Sb 3d 5/2	Sb 3d 3/2	S 2p 3/2	S 2p ½
Peak position (eV)	529.72	539.08	161.57	162.81
FWHM (eV)	0.95	0.95	0.94	0.94
Area	64530.09	42589.86	7604.04	3802.02
Sb_2O_3 (from bulk)	Sb 3d 5/2	Sb 3d 3/2		
Peak position (eV)	530.54	539.79		
FWHM (eV)	1.04	1.04		
Area	17096.58	11283.74		
Sb_2O_5 (from bulk)	Sb 3d 5/2	Sb 3d 3/2		
Peak position (eV)	531.63	540.89		
FWHM (eV)	0.92	0.92		
Area	6346.11	4188.43		

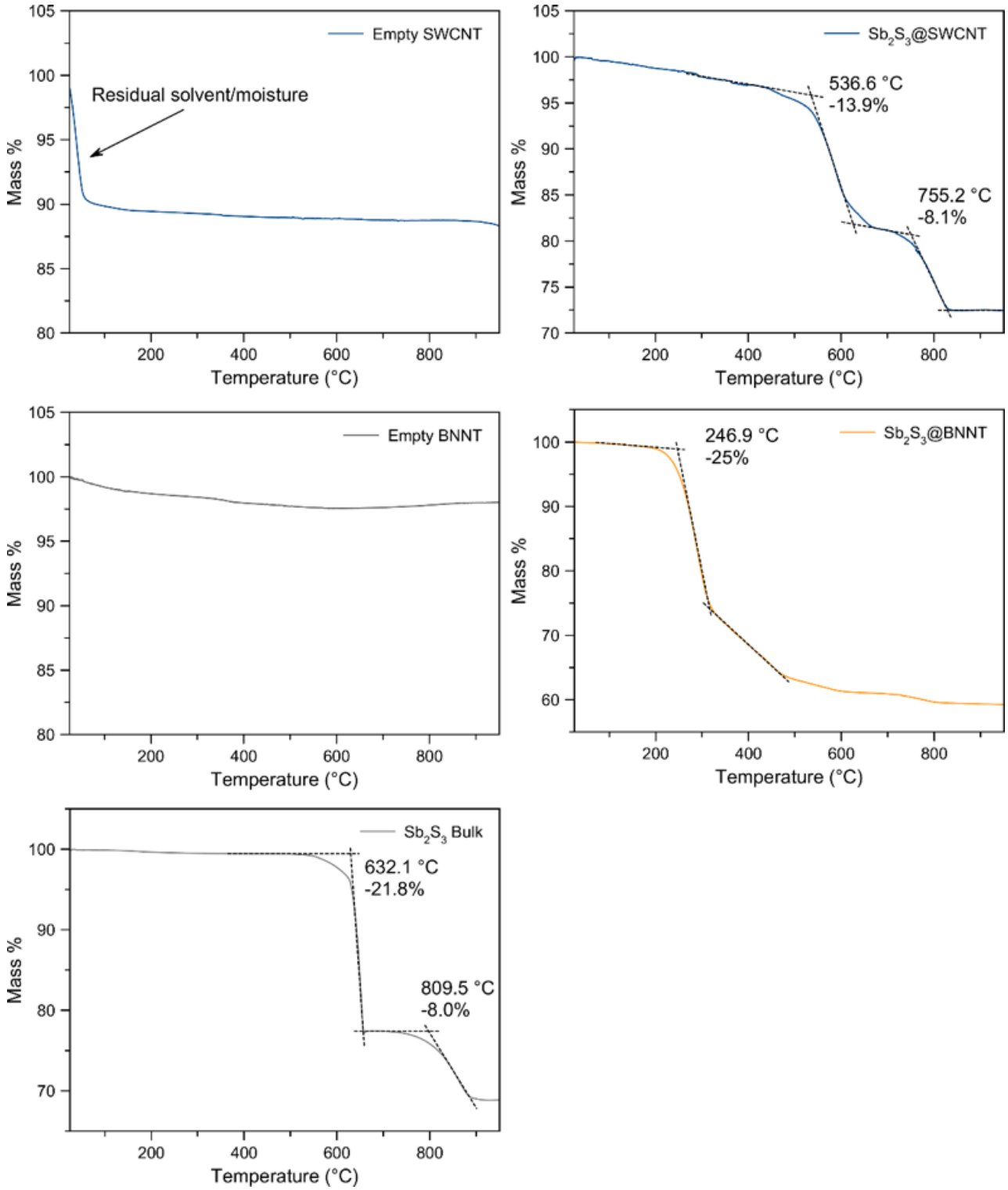

Figure S11. TGA curves of SWCNTs, c-Sb_2S_3@SWCNTs, BNNTs, a-Sb_2S_3@BNNTs, and bulk Sb_2S_3 with nitrogen purge.

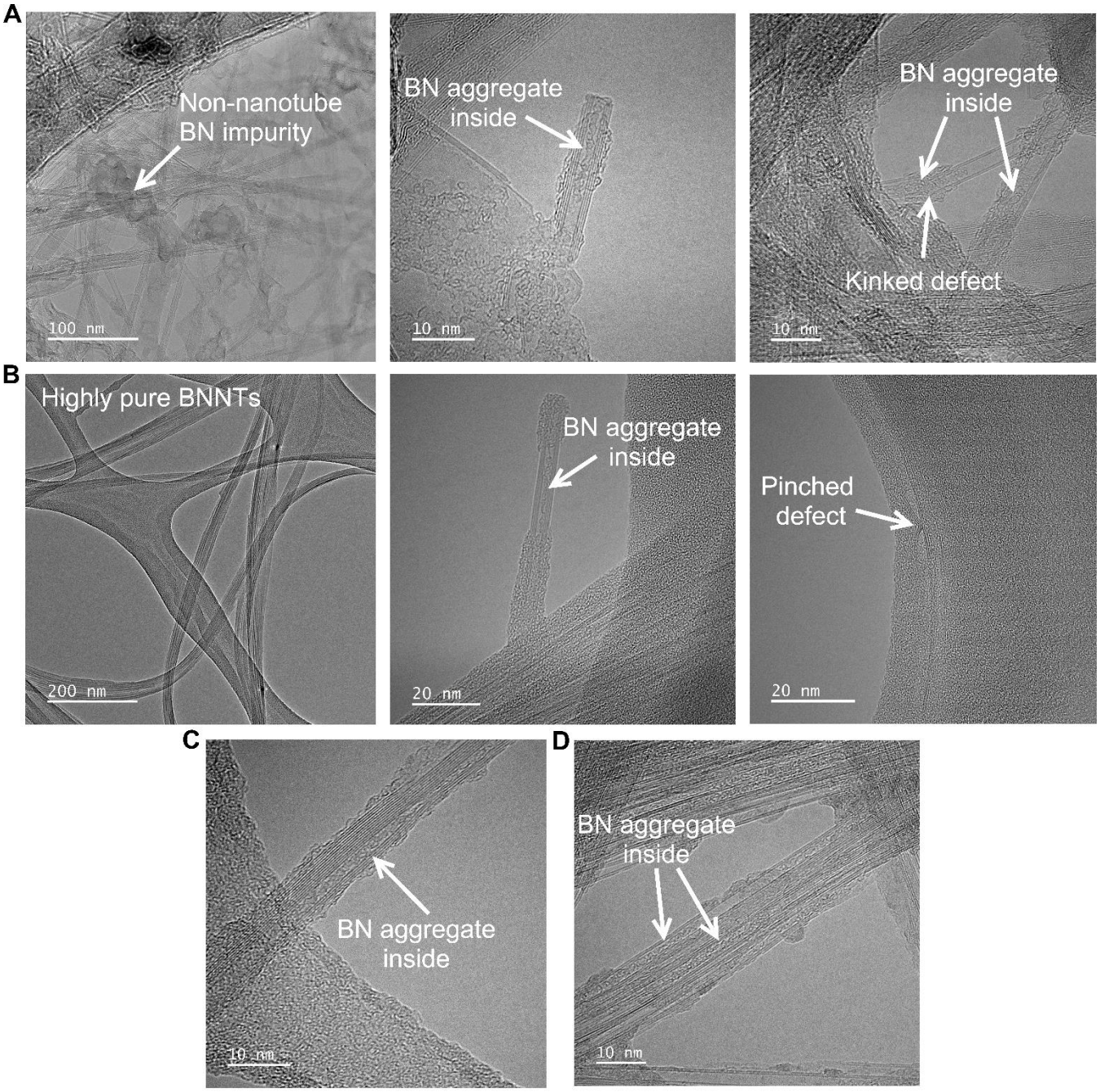

Figure S12. Representative HRTEM images of empty BNNTs. (A) Purified and treated (to open ends) BNNTs, which contained defects, BN aggregate filling within BNNTs, and a high quantity of non-nanotube BN outside of the nanotubes. (B) High purity BNNTs exposed to a proprietary purification process (BNNT LLC) much longer than the nanotubes used in this study with no non-nanotube material remaining outside the BNNTs. BN aggregates remained inside the nanotubes. (C) High purity nanotubes from B which were additionally exposed to calcination at 800 ^{o}C for 5 hours, after which BN aggregate filling remained. (D) High purity nanotubes from B which were first washed in aqua regia for 5 hours and subsequently washed thoroughly with water followed by calcination at 800 ^{o}C for 5 hours. BN aggregate filling remained after this process. These aggregates likely act as a defect and is responsible for a significant portion of the Sb_2S_3-filled samples being a-Sb_2S_3.

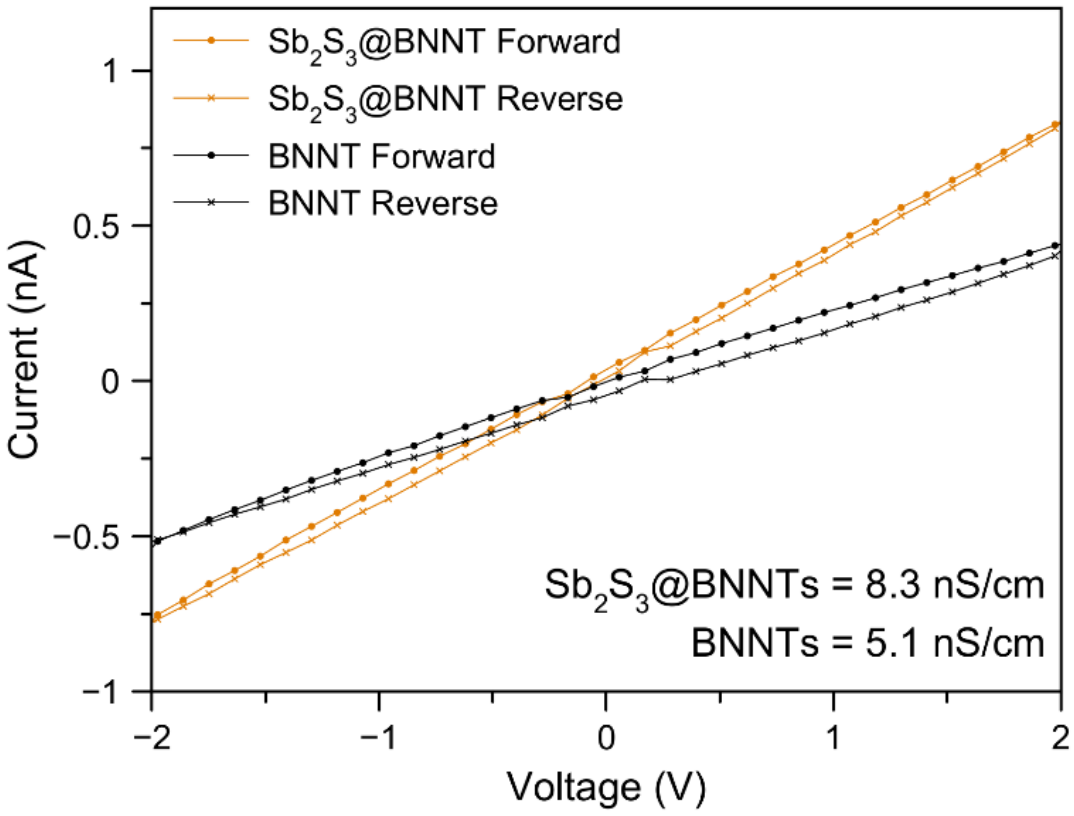

Figure S13. Conductivity measurements of Sb_2S_3@BNNT and BNNT pressed pellets. Sb_2S_3@BNNT: l=0.168 cm, A=0.269 x 0.0295 cm = 0.00796 cm^2; empty BNNT: l=0.136 A=0.264 x 0.0242 cm = 0.00637 cm^2

References

(1)Hanwell, M. D.; Curtis, D. E.; Lonie, D. C.; Vandermeersch, T.; Zurek, E.; Hutchison, G. R. Avogadro: An Advanced Semantic Chemical Editor, Visualization, and Analysis Platform. *J. Cheminformatics* **2012**, *4* (1), 17. https://doi.org/10.1186/1758-2946-4-17.

(2)Humphrey, W.; Dalke, A.; Schulten, K. VMD: Visual Molecular Dynamics. *J. Mol. Graph.* **1996**, *14* (1), 33–38, 27–28. https://doi.org/10.1016/0263-7855(96)00018-5.

(3)Bayliss, P.; Nowacki, W. Refinement of the Crystal Structure of Stibnite, Sb_2S_3. *Z. Für Krist.* **1972**, *135* (3–4), 308–315. https://doi.org/10.1524/zkri.1972.135.3-4.308.

(4)Schindelin, J.; Arganda-Carreras, I.; Frise, E.; Kaynig, V.; Longair, M.; Pietzsch, T.; Preibisch, S.; Rueden, C.; Saalfeld, S.; Schmid, B.; Tinevez, J.-Y.; White, D. J.; Hartenstein, V.; Eliceiri, K.; Tomancak, P.; Cardona, A. Fiji: An Open-Source Platform for Biological-Image Analysis. *Nat. Methods* **2012**, *9* (7), 676–682. https://doi.org/10.1038/nmeth.2019.

(5)Peters, J. J. P. A Fast Frozen Phonon Algorithm Using Mixed Static Potentials. *Ultramicroscopy* **2021**, *229*, 113364. https://doi.org/10.1016/j.ultramic.2021.113364.

(6)Duncan, D. R. The Colour of Pigment Mixtures. *Proc. Phys. Soc.* **1940**, *52* (3), 390. https://doi.org/10.1088/0959-5309/52/3/310.

(7)Clark, S. J.; Segall, M. D.; Pickard, C. J.; Hasnip, P. J.; Probert, M. I. J.; Refson, K.; Payne, M. C. First Principles Methods Using CASTEP. *Z. Für Krist. - Cryst. Mater.* **2005**, *220* (5–6), 567–570. https://doi.org/10.1524/zkri.220.5.567.65075.

(8)Perdew, J. P.; Burke, K.; Ernzerhof, M. Generalized Gradient Approximation Made Simple. *Phys. Rev. Lett.* **1996**, *77* (18), 3865–3868. https://doi.org/10.1103/PhysRevLett.77.3865.

(9)Grimme, S. Semiempirical GGA-type density functional constructed with a long-range dispersion correction. *J. Comput. Chem.* **2006**, *27* (15), 1787–1799. https://doi.org/10.1002/jcc.20495.

(10)Sanville, E.; Kenny, S. D.; Smith, R.; Henkelman, G. Improved grid-based algorithm for Bader charge allocation. *J. Comput. Chem.* **2007**, *28* (5), 899–908. https://doi.org/10.1002/jcc.20575.

(11)Tang, W.; Sanville, E.; Henkelman, G. A Grid-Based Bader Analysis Algorithm without Lattice Bias. *J. Phys. Condens. Matter* **2009**, *21* (8), 084204. https://doi.org/10.1088/0953-8984/21/8/084204.

(12) Biesinger, M. C. Accessing the Robustness of Adventitious Carbon for Charge Referencing (Correction) Purposes in XPS Analysis: Insights from a Multi-User Facility Data Review. *Applied Surface Science* **2022**, 597, 153681. https://doi.org/10.1016/j.apsusc.2022.153681.